Dynamical instability of a spin spiral in an interacting Fermi gas as a probe of the Stoner transition

G.J. Conduit[1, 2, *] and E. Altman[1]

[1]*Department of Condensed Matter Physics, Weizmann Institute of Science, Rehovot, 76100, Israel*
[2]*Physics Department, Ben Gurion University, Beer Sheva, 84105, Israel*
(Dated: July 14, 2010)

We propose an experiment to probe ferromagnetic phenomena in an ultracold Fermi gas, while alleviating the sensitivity to three-body loss and competing many-body instabilities. The system is initialized in a small pitch spin spiral, which becomes unstable in the presence of repulsive interactions. To linear order the exponentially growing collective modes exhibit critical slowing down close to the Stoner transition point. Also, to this order, the dynamics are identical on the paramagnetic and ferromagnetic sides of the transition. However, we show that scattering off the exponentially growing modes qualitatively alters the collective mode structure. The critical slowing down is eliminated and in its place a new unstable branch develops at large wave vectors. Furthermore, long-wavelength instabilities are quenched on the paramagnetic side of the transition. We study the experimental observation of the instabilities, specifically addressing the trapping geometry and how phase-contrast imaging will reveal the emerging domain structure. These probes of the dynamical phenomena could allow experiments to detect the transition point and distinguish between the paramagnetic and ferromagnetic regimes.

I. INTRODUCTION

A magnetic field tuned Feshbach resonance provides a powerful tool to control the interaction parameters of ultracold atomic Fermi gases [1]. The effective interaction between two atoms in an s-wave scattering channel is attractive on one side of the resonance and repulsive on the other side, with both regimes diverging upon approaching the resonance. Over the last few years experiments starting from the attractive side have investigated the crossover from a Bardeen-Cooper-Schrieffer state of fermion pairs to a Bose-Einstein condensate of tightly bound molecules [2]. On the other hand, a recent experiment has provided the first possible evidence for a transition to an itinerant ferromagnet beyond a critical interaction strength in the repulsive regime [3]. If confirmed, this new realization of ferromagnetism may not only resolve long-standing questions stemming from the solid state but also promises to open up new arenas of ferromagnetism research [4–8].

When considering the repulsive side of the resonance however, it must be noted that the repulsive Fermi gas is only a meta-stable state. The two-body ground state in this regime is a "Feshbach molecule", a bound state with negative energy. Correspondingly, the many fermion ground state is the molecular BEC, whereas the repulsive Fermi gas arises only if the system is specially prepared without molecules. Even then, atoms gradually recombine to form Feshbach molecules. At least in the low density limit, this occurs predominantly through a three-body process [9], whereas closer to the resonance the loss may reflect competing many-body instabilities [10]. An experiment as in Ref. [3] must therefore be performed inherently out of equilibrium. To abate the fall in atom density the experiment was performed while tuning the

interaction parameter rapidly, but this however masks the true phase transition [11, 12]. Moreover, it has been shown that even if the atom number is kept constant by coupling the system to an atom reservoir, the non-equilibrium conditions imposed by the three-body loss act to change the nature of the ferromagnetic transition through an inherently quantum mechanism [13].

In this paper we propose a different strategy to investigate the Stoner transition, which could allow investigators to circumvent the difficulties imposed by atom loss. The idea is to study the dynamical stability of a nearly ferromagnetic state, or more precisely a spin spiral of small wave-vector $\mathbf{Q}$, as shown in Fig. 1(b). This state has minimal three-body losses as it is locally fully polarized. On the other hand, the dynamical stability of the spiral spin texture is not protected by spin conservation because the system has zero net magnetization. To take advantage of this new protocol it is first vital to determine how the modes of instability change when we tune the system across the Stoner transition. For an interaction strength tuned so that ferromagnetism is favored, the exponentially growing unstable modes are expected to reorient the spins, as seen in Fig. 1(c), and eventually cause the system to fragment into polarized domains. A similar collective modes structure was observed in a bosonic ferromagnetic gas [14]. Unlike when ordering from the paramagnetic state [11], the size of these domains and the collective mode structure can be finely tuned with the length scale of the initial spin spiral.

On approaching the Stoner transition we find critical slowing down of the unstable modes. However, counter to initial heuristic expectations, the unstable modes of the helical spin state are, to linear order, the same on the two sides of the transition. To differentiate between the ferromagnetic and paramagnetic regimes we go beyond the
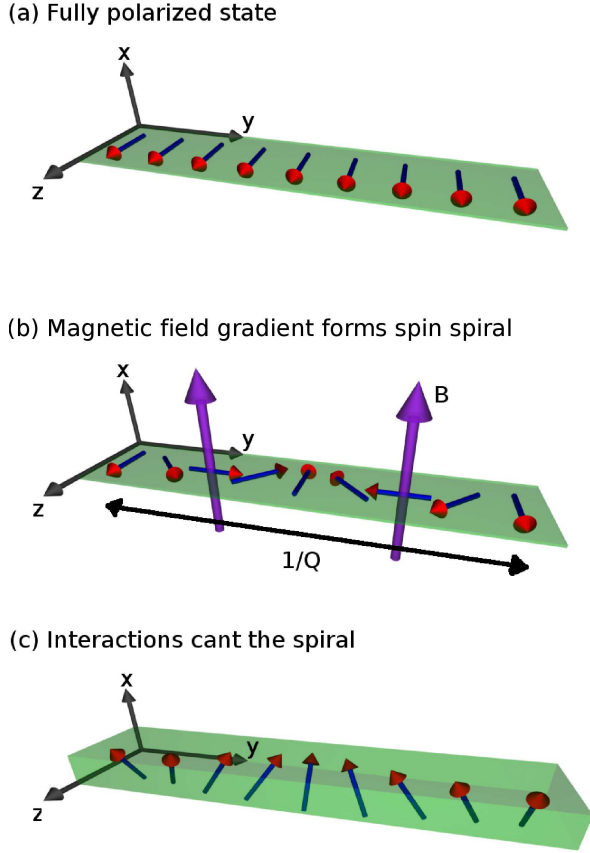
(a) Fully polarized state

(b) Magnetic field gradient forms spin spiral

(c) Interactions cant the spiral

FIG. 1: (Color online) (a) The gas is started in a fully polarized state and (b) a normal magnetic field B (purple arrows) is applied to form a spin spiral of pitch $1/Q$. When the interaction strength is ramped upwards (c) the spins rotate into the y direction forming a fully polarized state (which we later show has a long wavelength modulation). The thickness of the green plane indicates the growing magnetization. In (b) and (c) the axis basis set co-rotates with the spin spiral.

linear analysis and study the feedback effect due to the scattering of collective excitations off the exponentially growing modes. As the phenomena investigated are not only of conceptual interest but could also provide a new protocol for the next generation of experiments, we also consider the ramifications of a realistic harmonic trapping potential and the experimental probes of the collective modes.

II. FORMING THE SPIN SPIRAL

To form the initial spin spiral, the atomic gas is first prepared in a fully polarized phase, say along the z spin axis shown in Fig. 1(a), and a magnetic field gradient is imposed perpendicular to the magnetization axis (e.g. $\mathbf{B} = by\hat{\mathbf{x}}$) for time t. Such a field can be thought of as a gradient of the relative potential between the $\uparrow_x$ and $\downarrow_x$ spins, and leads to a (constant) relative acceleration between these two spin components in the coherent

spin state. The result is a spiral spin texture, as shown in Fig. 1(b), with wave vector $Q_y = (\mu_B g_J t/\hbar)dB_x/dy$, where g_J is the g-factor. The twist rate is independent of the spin stiffness and the strength of the repulsive interactions between particles. This is in close analogy to the effect of a potential gradient placed across a superfluid, which is essentially a XY ("phase") ferromagnet. The potential gradient affects phase twist at a constant rate, independent of the superfluid stiffness, which corresponds to free acceleration according to Newton's law.

To gain further understanding into why interactions do not impact on the dynamic formation of the initial spin spiral we can study the system within the simple setting of the Heisenberg ferromagnet. Then, the situation posed in Fig. 1 is described by the Hamiltonian $\hat{H} = -J\sum_{\langle ij \rangle} \hat{\mathbf{S}}_i \cdot \hat{\mathbf{S}}_j - b\sum_i y_i \hat{S}_i^x$, where the first summation covers nearest neighbors on the lattice, J denotes the coupling between adjacent sites, and b is the magnetic field gradient. The initial conditions are $S_i^x(t=0) = 0$, $S_i^y(t=0) = 0$, and $S_i^z(t=0) = S_0$. We then study the evolution of the spins using $\hbar\dot{\mathbf{S}} = i[\hat{H}, \mathbf{S}]$, finding the equations of motion $\hbar\dot{S}_{x,i} = 0$, $\hbar\dot{S}_{y,i} = by_i S_{z,i}$, and $\hbar\dot{S}_{z,i} = -by_i S_{y,i}$, where the components containing J cancel exactly. Finally, we can then solve the equations of motion to yield $S_{x,i}(t) = 0$, $S_{y,i}(t) = S_0 \sin(by_i t/\hbar)$, and $S_{z,i}(t) = S_0 \cos(by_i t/\hbar)$. These show that the formation of the spin spiral by the external magnetic field gradient is independent of the interactions, J, between particles.

An interesting and beneficial practical implication of the above observation is to alleviate the need to first form a spiral, and then perform a Feshbach field quench. The spin spiral may equally well be formed with the Feshbach field in place. Finally we note that a magnetic field gradient has the side effect of imparting a translational force on the gas perpendicular to the gradient. Fortunately, in this scheme we need to impose only a long-pitched spin spiral, which requires only a weak magnetic field gradient with minimal side effect.

Following the preparation stage, we are ready to allow the spiral state to evolve under the influence of the repulsive interactions tuned by the Feshbach field, and track its evolution into the polarized state out of the plane of the initial spiral shown in Fig. 1(c).

III. LINEAR SPIN-WAVE INSTABILITY

We now investigate the instabilities of the helical spin state by first focusing on the linearized spin fluctuations around the initial spin spiral. The exponentially growing unstable modes will show up in this analysis as collective excitations with imaginary frequencies. As the dominant modes grow exponentially, non-linear processes become important. Later in Sec. IV we will study how scattering off the exponentially growing modes renormalizes the spectrum.

To study the collective modes we start from the quantum partition function expressed as a fermionic coherent state path integral, $\mathcal{Z} = \mathrm{Tr}\, e^{-\beta(\hat{H} - \mu\hat{N})} = \int \mathcal{D}\psi e^{-S}$, with the corresponding action

$$S = \int \sum_{\sigma=\{\uparrow,\downarrow\}} \bar{\psi}_\sigma \left(\partial_\tau + \epsilon_{\hat{\mathbf{k}}} - \mu\right)\psi_\sigma + \int g\bar{\psi}_\uparrow\bar{\psi}_\downarrow\psi_\downarrow\psi_\uparrow, \quad (1)$$

where $\int \equiv \int_0^\beta d\tau \int d\mathbf{r}$, the free particle dispersion is $\epsilon_{\mathbf{k}} = k^2/2$, μ is the chemical potential, and $g\delta^3(\mathbf{r})$ is the strength of the s-wave repulsive contact interaction. We have also set $\hbar = m = 1$. To explore how interactions impinge on the collective mode spectrum we affect a Hubbard-Stratonovich decoupling, which incorporates the spin channels $\phi_0 + \phi$ [6, 15]. The static component of the magnetization, ϕ_0, follows the initial helical spatial spin texture and ϕ represents the growing unstable modes and fluctuations around that stationary component. It is also convenient to apply a gauge transformation $\psi \mapsto \psi e^{i\mathbf{Q}\cdot\mathbf{r}\sigma_x/2}$ to enter a spatially rotating basis set with pitch vector $Q\mathbf{e}_x/2$, which renders the initial spin texture, and thus also the static component of the magnetization to be uniform, $\phi_0 = (0,0,\phi_0)$.

After integrating out the Grassmann fields we obtain $\mathcal{Z} = \int \mathcal{D}\phi e^{-S}$ with the action

$$S = \int g\phi_0^2 - \mathrm{Tr}\ln\left(\hat{\mathsf{G}}_0^{-1}\right)$$
$$+ \int g\phi^2 - \mathrm{Tr}\ln\left[\mathsf{I} + \hat{\mathsf{G}}_0\left(\frac{1}{2}\sigma_x\mathbf{Q}\cdot\hat{\mathbf{k}} - g\boldsymbol{\sigma}\cdot\phi\right)\right], \quad (2)$$

where $\hat{\mathsf{G}}_0^{-1} = \partial_\tau + \epsilon_{\hat{\mathbf{k}}} - \mu - g\sigma_z\phi_0 = \hat{G}_{\sigma_z}^{-1}$ denotes the elements of the inverse Green function at the level of the renormalized mean field. We then expand in the perturbative collective modes ϕ. We assume that the initial spin spiral has a long wavelength relative to the Fermi wave vector k_F, so we work in the regime $Q \ll k_F$. Focusing on the soft modes that are perpendicular to the saddle point field, the dispersion satisfies $\omega \ll \mu$ and has wave vector $q \ll k_F$. Following the expansion for the soft modes we get the contribution to the action from fluctuations

$$S = \int g(\phi_x^2 + \phi_y^2)$$
$$+ \mathrm{Tr}\left\{\hat{G}_+\left[\frac{\mathbf{Q}\cdot\mathbf{k}}{2} - g(\phi_x - i\phi_y)\right]\hat{G}_-\left[\frac{\mathbf{Q}\cdot\mathbf{k}}{2} - g(\phi_x + i\phi_y)\right]\right\}$$
$$+ \frac{1}{2}\mathrm{Tr}\left\{\hat{G}_+\left[\frac{\mathbf{Q}\cdot\mathbf{k}}{2} - g(\phi_x - i\phi_y)\right]\hat{G}_-\left[\frac{\mathbf{Q}\cdot\mathbf{k}}{2} - g(\phi_x + i\phi_y)\right]\right\}^2. \quad (3)$$

Before searching for the collective modes it is useful to transform the basis set for the magnetization from Cartesian to spherical polar coordinates: $\phi = \phi_0[1 + \eta](\cos\theta, \sin\theta\sin\varphi, \sin\theta\cos\varphi)$. Note that θ is defined as the angle with respect to the positive x axis, and φ is the angle from the z axis of the projection of ϕ onto the

y,z plane. The initial state is $\theta = \pi/2$ and $\varphi = 0$, which ensures that fluctuations in φ are well defined. With this definition we expand in small thermal and quantum fluctuations away from the fully polarized state that are both angular φ and θ (now redefined to be centered around $\pi/2$), and also in the amplitude of the mode, η. The perturbative form for the expansion correct to quadratic order is $\phi = \phi_0[1+\eta](-\theta, \varphi, 1-[\theta^2+\varphi^2]/2)$. Although both Cartesian and spherical polar basis sets yield the same collective mode structure in this linear response analysis, when in Sec. IV we consider feedback corrections to this response it will be necessary to work with the spherical polar basis set to properly evaluate phase and amplitude fluctuations. However, to study the system with only linear response we also expand $G_\pm$ in ω and $\mathbf{q}$ and find that the soft modes are coupled in the action through

$$S = S_0\,\mathrm{Tr}\left\{\begin{pmatrix}\theta_{-\mathbf{q}}^{-\omega} & \varphi_{-\mathbf{q}}^{-\omega}\end{pmatrix}\begin{pmatrix}\chi[q^2 - Q^2] & i\omega \\ -i\omega & \chi q^2\end{pmatrix}\begin{pmatrix}\theta_{\mathbf{q}}^\omega \\ \varphi_{\mathbf{q}}^\omega\end{pmatrix}\right\}, \quad (4)$$

where $\chi = \frac{1}{2} - \frac{2^{2/3}3}{5k_Fa}$, $q^2 = q_x^2 + q_y^2 + q_z^2$, and $S_0 = 2^{1/3}\beta\phi_0 k_F a/\pi$. The twist wave vector Q couples only to the magnetization along the initial spin spiral. Due to their commutation relations, the conjugate modes are coupled by the off-diagonal elements and so to extract the dispersion we demand that the determinant of the matrix is zero. This yields the dispersion

$$\omega = \pm\chi q\sqrt{q^2 - Q^2}, \quad (5)$$

which is shown in Fig. 2(a). We first verify the dispersion in the absence of the spin spiral. When $Q = 0$ and interactions are strong so $\chi \to 1/2$ we recover the familiar dispersion of a single particle, $\omega = q^2/2$. When $q < Q$ the dispersion is imaginary, corresponding to an instability, whereas when $q > Q$ we recover oscillating modes. Note that, as required by spin conservation, there is no dynamical instability of the magnetization at zero wavevector. Similarly growth at $q = Q$ is stunted as this mode is initially fully polarized. The exponential growth of the order parameter is maximal at the wave-vector $q = Q/\sqrt{2}$, and it is at this length scale that we would expect to see ferromagnetic domains emerge. In the experiment [3] domain walls could not be observed in a gas starting from a paramagnetic state since their size falls below the resolution of current experimental techniques [11], but here their length scale can be tuned to be experimentally observable by changing the pitch of the spin spiral. The fully polarized phase becomes unstable at the critical interaction strength $k_Fa = 2^{5/3}3/5 \approx 1.90$. At this interaction strength $\chi = 0$ so the system undergoes critical slowing and the characteristic time of the instability diverges.

Against intuitive expectations we find the same collective mode structure, to linear order, on either side of the transition. To gain insight on this, it is useful to study the linear stability of a spiral texture in the Heisenberg model on a lattice $\hat{H} = -J\sum_{\langle ij\rangle}\hat{\mathbf{S}}_i\cdot\hat{\mathbf{S}}_j$. Here $\langle ij\rangle$ restricts the summation to nearest neighbors and J denotes

the coupling between adjacent sites. A straightforward spin wave analysis of the fluctuations about the spiral texture yields the collective mode dispersion

$$\omega_{\mathrm{H}} = 4JS\sqrt{\cos^2(Qa)\sin^2\!\left(\frac{q_{\mathrm{x}}a}{2}\right)+\sin^2\!\left(\frac{q_{\mathrm{y}}a}{2}\right)+\sin^2\!\left(\frac{q_{\mathrm{z}}a}{2}\right)}$$
$$\times\sqrt{\sin^2\!\left(\frac{q_{\mathrm{x}}a}{2}\right)+\sin^2\!\left(\frac{q_{\mathrm{y}}a}{2}\right)+\sin^2\!\left(\frac{q_{\mathrm{z}}a}{2}\right)-\sin^2\!\left(\frac{Qa}{2}\right)}, \quad (6)$$

where a is the lattice spacing. Note that in the limit $qa \ll 1$ and $Qa \ll 1$ the collective mode dispersion Eq. (6) computed in the Heisenberg model approaches the same form Eq. (5) developed in the continuum case. Tuning the coupling from ferromagnetic to antiferromagnetic through criticality at $J = 0$ is allied with a vanishing dis[persion, as found at the Stoner transition of the Fermi system. The anisotropy introduced by the first root gives a preference to modes with a wave vector in the plane of the spiral.

We note that the equivalent dynamics of the initial spin-spiral seen for positive and negative J is due to an exact symmetry of the Heisenberg Hamiltonian. This can be shown by a variation on the arguments presented in Ref. [16], which is valid for initial states invariant under some generalized time reversal transformation. Such an exact symmetry does not exist in the itinerant fermion model of interest here. Rather the symmetry of the collective mode dispersion around the dynamical critical point is an emergent phenomenon, and as we shall see later in Sec. IV, valid only within the linear approximation of the dynamics.

Before proceeding to study these nonlinear effects, we revisit our initial assumption that the three-body loss may be neglected in the proposed setup. To assess the validity of this assumption we shall compare the loss rate in the spin spiral to the growth rate of the maximally unstable mode around this spiral state. The three-body loss rate (strictly valid for $k_{\mathrm{F}}a \ll 1$) is $111\bar{\epsilon}(k_{\mathrm{F}}a)^6 n_\uparrow n_\downarrow(n_\uparrow + n_\downarrow)$ [9]. To evaluate this we note that adjacent spins in the spiral, separated by $r_{\mathrm{s}} = (2/9\pi)^{1/3}k_{\mathrm{F}}^{-1}$, have an angle between them of $Qr_{\mathrm{s}} \ll 1$. Therefore the adjacent spins give a geometric component of $n_\uparrow n_\downarrow = (2/9\pi)^{2/3}n^2(Q/k_{\mathrm{F}})^2/4$. Applying this to the experimental regime gives the loss rate $0.12(k_{\mathrm{F}}a)^6(Q/k_{\mathrm{F}})^2\,\mathrm{s}^{-1}$.

On the other hand, the growth rate of the dominant mode, according to Eq. (5), is $\max_{\mathbf{q}}\{\mathrm{Im}[\omega(\mathbf{q})]\} = (1 - 2^{5/3}3/5k_{\mathrm{F}}a)Q^2/4$. Interestingly we observe that the ratio of loss to growth rate depends only on the interaction strength and not on the spiral pitch Q. Comparing the two rates we find that the loss will dominate for strong interactions $k_{\mathrm{F}}a \gtrsim 4.9$, though in this regime the formula for loss rate significantly overestimates the true loss [17] and in fact the theory should be valid for even higher interaction strengths. However, in the experimentally accessible region including the phase transition,

$k_{\mathrm{F}}a < 2.5$, loss is more than 60 times smaller than the dominant growth rate of the collective modes. Therefore the new experimental protocol offers a promising way to observe magnetism without the damaging effects of loss. In addition, losses will dominate within a small region of width $\delta(k_{\mathrm{F}}a) \sim 0.03$ surrounding the point of critical slowing down. However, we shall see in the next section that non-linear feedback effects drive a new dynamical instability at large wave-vectors precisely in the region of critical slowing down, and that this instability will overcome the losses.

IV. NONLINEAR COLLECTIVE MODES

In the previous section we found that the behavior of the collective modes spectrum with interaction strength is qualitatively similar either side of the critical interaction strength $k_{\mathrm{F}}a = 2^{5/3}3/5$. However, for the Fermi system this is only a feature of the linear analysis, which we now extend to include, self-consistently, the effect of the scattering of fluctuations on the exponentially growing modes. We will see that this mechanism also eliminates the region of critical slowing down by generating new unstable modes at high wave-vectors near to the critical interaction strength.

We focus solely on the consequences of scattering off a single dominant growth mode $\Phi_{\mathbf{P}}$. According to the analysis of Sec. III, the momentum $\mathbf{P}$ associated with the dominant mode is $Q/\sqrt{2}$, though here we allow a general wave vector that we will later determine self consistently. In presence of the large mode $\Phi_{\mathbf{P}}$, we have to expand the action Eq. (2) to cubic order to include terms which are linear in $\Phi_{\mathbf{P}}$ and quadratic in the other modes

$$S_\Phi = \int g^3 \,\mathrm{Tr}\left[G_-(\Phi_{\mathrm{x}} + \mathrm{i}\Phi_{\mathrm{y}})G_+\phi_{\mathrm{z}}G_+(\phi_{\mathrm{x}} - \mathrm{i}\phi_{\mathrm{y}})\right.$$
$$\left. - G_+(\Phi_{\mathrm{x}} - \mathrm{i}\Phi_{\mathrm{y}})G_-\phi_{\mathrm{z}}G_-(\phi_{\mathrm{x}} + \mathrm{i}\phi_{\mathrm{y}})\right], \quad (7)$$

where $G_\pm = \partial_\tau + \epsilon_{\hat{\mathbf{k}}} - \mu \mp g\phi_0$. This new scattering mechanism couples the $\{\phi_{\mathrm{x}}, \phi_{\mathrm{y}}\}$ channels to the ϕ_{z} channel, and so describes scattering out of the original magnetization configuration and into the dominant growing mode. The presence of a growing classical field $\Phi(t) = \Phi(0)e^{\mathrm{i}\Omega\tau}$ (with imaginary frequency Ω), requires a seed fluctuation in the initial spiral state. Such a seed will be present in any realistic implementation because of random inhomogeneity in the magnetic field and thermal fluctuations.

We again transform to the spherical polar basis set to properly separate phase and amplitude fluctuations. Coupling to the exponentially growing mode of wave vector $\mathbf{P}$ and frequency Ω requires studying the spin susceptibility matrix expanded out to include couplings between other modes at wave vectors $\mathbf{q}$ and $\mathbf{q}\pm\mathbf{P}$, and frequencies ω and $\omega \pm \Omega$. The coupled action then takes the form
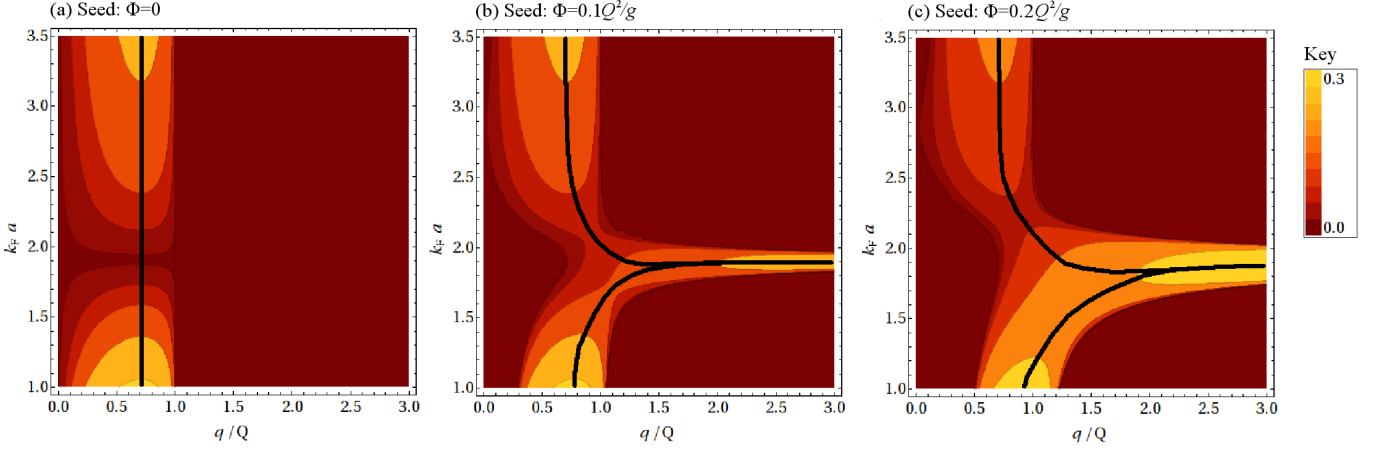
FIG. 2: (Color online) The variation of the exponential growth rate of the collective mode at wave vector $\mathbf{q}$ with interaction strength $k_{\mathrm{F}}a$. Calculated for an initial seed field of size (a) $\Phi = 0$, (b) $\Phi = 0.1Q^2/g$, and (c) $\Phi = 0.2Q^2/g$. The fields $\{\theta, \varphi\}$ are evaluated at wave vector $\mathbf{q}$, and η at wave vector $\mathbf{q} \pm \mathbf{Q}$; we focus on the peak contribution to the growth with $\mathbf{q} \parallel \mathbf{Q}$. The black trajectory highlights the maximum growth rate at a given interaction strength.

$$S = S_0 \, \mathrm{Tr} \left\{ \begin{pmatrix} \theta_{-\mathbf{q}}^{-\omega} & \varphi_{-\mathbf{q}}^{-\omega} & \eta_{-\mathbf{q}-\mathbf{P}}^{-\omega-\Omega} & \eta_{-\mathbf{q}+\mathbf{P}}^{-\omega+\Omega} \end{pmatrix} \begin{pmatrix} \chi[q^2-Q^2] & i\omega & \zeta & \zeta \\ -i\omega & \chi q^2 & \zeta & \zeta \\ \zeta & \zeta & \frac{3E_{\mathrm{F}}}{2}\left[\chi - \frac{\pi(\omega+\Omega)}{\sqrt{2E_{\mathrm{F}}}|\mathbf{q}+\mathbf{P}|}\right] & 0 \\ \zeta & \zeta & 0 & \frac{3E_{\mathrm{F}}}{2}\left[\chi - \frac{\pi(\omega-\Omega)}{\sqrt{2E_{\mathrm{F}}}|\mathbf{q}-\mathbf{P}|}\right] \end{pmatrix} \begin{pmatrix} \theta_{\mathbf{q}}^{\omega} \\ \varphi_{\mathbf{q}}^{\omega} \\ \eta_{\mathbf{q}+\mathbf{P}}^{\omega+\Omega} \\ \eta_{\mathbf{q}-\mathbf{P}}^{\omega-\Omega} \end{pmatrix} \right\}, \quad (8)$$

where $\zeta = 3E_{\mathrm{F}}\theta_{\mathrm{s}}(1 - \frac{2^{2/3}g}{5k_{\mathrm{F}}a})/2$, E_{F} is the polarized state Fermi energy, and θ_{s} denotes the seed field size for either θ or φ. The expansion in frequencies employed for the amplitude modes, η, applies for $\omega \ll q$, which holds for the regime of interest that describes the coupling the soft angular modes to the amplitude modes. We again search for the zeros in the resultant determinant to extract the collective modes and explore the unstable region. Note that in the absence of the growing field, the formalism immediately recovers the dispersion found in Sec. III. However, here we aim to go further and consider the form of the modes in the presence of the dominant growing field. To ensure that the formalism is self consistent at each interaction strength we first compute the feedback-corrected dominant mode before calculating the entire collective modes spectrum in the presence of that growing mode. We also note that this formalism respects the the spin conservation law, and so, as in the linear analysis of Sec. III, growth of the uniform component of the magnetization is suppressed.

The final result for the spectrum is shown in Fig. 2 for different values of the seed field. First we note that for interaction strengths far from the critical slowing, scattering on the growing mode is negligible. In particular the dominant growth mode remains at $\sim Q/\sqrt{2}$ in this regime. However, near to critical slowing the wave vector of the dominant growth mode can be enhanced. This can

be understood by comparing the on and off-diagonal elements of the action matrix, Eq. (8). Upon nearing critical slowing, the on-diagonal elements, being proportional to χ, approach zero. However, the off-diagonal terms, ζ, that represent scattering off the dominant growing modes are non-zero. To ensure that the overall determinant is zero demands a non-zero value for the on-diagonal elements which requires a large wave vector. On approaching critical slowing this growth in the wave vector would only be curtailed by higher order momentum terms. A detailed analysis shows that the wave vector of the peak growth tracks the trajectory along the critical slowing at $k_{\mathrm{F}}a = 2^{5/3}3/5$ in the phase diagram Fig. 2. The peak growth at a particular wave vector $\mathbf{q}$ is when that wave vector $\mathbf{q}$ is parallel to the direction of $\mathbf{Q}$, and so we focus on that contribution in Fig. 2. On the paramagnetic side of the resonance, $k_{\mathrm{F}}a < 2^{5/3}3/5$, the enhanced scattering into the higher momentum sector removes long wavelength components of the domains, whereas on the ferromagnetic side of the resonance, $k_{\mathrm{F}}a > 2^{5/3}3/5$, the larger domains are naturally still favored. Therefore, consideration of the feedback of the exponentially growing field yields an additional collective mode structure that could experimentally distinguish between the two sides of the critical slowing interaction strength.

This picture was developed in the presence of just a single growing exponential mode, whereas in reality these
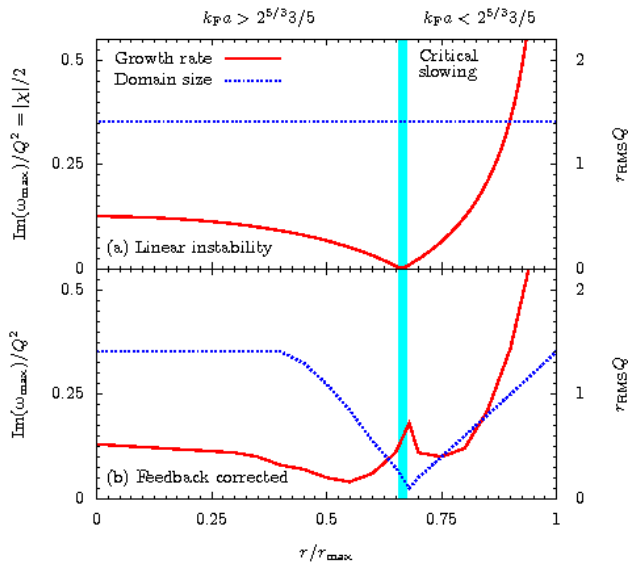
FIG. 3: (Color online) The variation of growth rate (red solid, primary y-axis) and domain size (blue dashed, secondary y-axis) with radius within a harmonic well. (a) corresponds to linear response, and when (b) feedback corrections with a seed field of size $0.2Q^2/g$ are taken into account. The vertical cyan line denotes the radius corresponding to critical slowing and $r_{\max}$ is the outer radius of the atom distribution.

seed modes have an initial growth rate $\sim \chi q\sqrt{Q^2 - q^2}$ (Eq. (5)) centered around the wave vector $q = Q/\sqrt{2}$ corresponding to maximal growth. With reference to Fig. 2, except near to critical slowing, at a given interaction strength the mode growth rate is sharply peaked as a function of q so that the presence of other less dominant exponentially growing modes blurs the collective modes dispersion by less than 5%. The relative initial size of those modes can however have an impact on the mode spectrum. Created by inhomogeneities in the applied magnetic field, the uncertainty can correspond to seeing a range of growth rates, for example the range spanning between Fig. 2(a) and Fig. 2(c). Though the growth rate around critical slowing is quantitatively different, the qualitative features are robust and the dominant growth wave vectors remain the same, so in the experiment strong signatures of ferromagnetism should be observed.

V. EXPERIMENTAL OBSERVATION

Having studied the instability to a ferromagnetic state in a uniform gas we now turn to consider the experimental ramifications of our results. We will focus on two key questions: first the consequences of the atomic gas being held within a realistic harmonic trapping potential, and second we address the experimental signatures of our predictions.

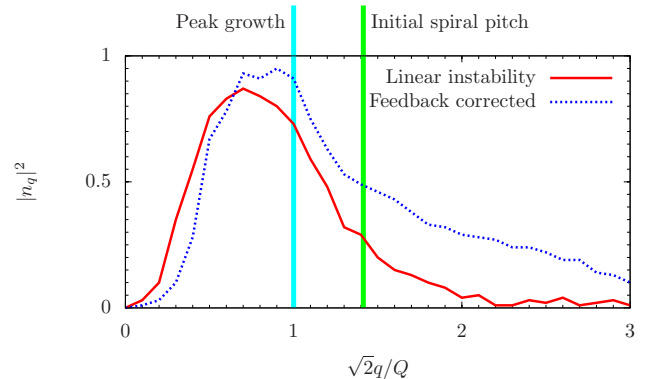We shall treat the harmonic confinement within the lo-

FIG. 4: (Color online) The Fourier transform of the domain distribution within a harmonic well. Without magnetization feedback is shown by the red solid line, and the blue dashed curve is in the presence of magnetization feedback. The peak growth rate at $Q/\sqrt{2}$ is labelled by the vertical cyan line, whereas the maximum growth wave vector Q is shown by the vertical green line.

cal density approximation. On passing radially outwards from the center of the harmonic well the local density and therefore the effective interaction strength falls. We can therefore use the results of the previous sections to map the rate at which the instability develops and its characteristic wavelength as a function of the radius. These results are shown in Fig. 3 for both the linear analysis (a) and when the feedback due to scattering on the growing mode is taken into account (b). Note significant modifications due to feedback corrections. First near the radius which corresponds to critical interactions there is a distinct maximum rather than a vanishing growth rate. The enhanced growth rate is driven by a scattering off the growing mode into large wave vectors. Therefore, secondly the characteristic wavelength of the unstable modes dips around that radius. In the linear analysis, by contrast the characteristic wavelength of the unstable modes is everywhere $2\pi\sqrt{2}/Q$.

We now turn to the question of how the distinct spatial structure of the instability may be observed in an experiment. The first approach we look at is to employ differential in-situ phase-contrast imaging, a method that has already been used on the ferromagnetic cold atom gas [3]. This measures the difference between the up and down-spin populations integrated along vertical columns through the gas. If the procedure is repeated across the gas, a two-dimensional map will be produced, which is governed by the pattern of the emergent magnetization aligned normal to the imaging plane. Once Fourier transformed, the spectrum of this map will reveal the typical magnetic domain size. To simulate the expected experimental result we employ a heuristic model of the gas. We divide the system into domains, with position dependent size, determined by the wavelength of the dominant growth mode at that radius. Each domain is then assigned either up or down magnetization at random,

and the resulting magnetization structure is column integrated to obtain a two dimensional magnetization image as in the experiment. The power spectrum of the domain structure in the simulated image is shown in Fig. 4. Without feedback corrections, according to Eq. (5) the dominant mode is at $q = Q/\sqrt{2}$ irrespective of interaction strength. In the numerical experiment a distinct peak exists at wave vectors around and below $Q/\sqrt{2}$; this is because adjacent domains were not necessarily misaligned thus increasing the effective length scale of the observed domains. If feedback corrections are taken into account then in the region of the trap corresponding to critical slowing significantly smaller domains are formed. This is reflected in the Fourier spectrum with reduced weight at small wave vectors, and enhanced weight at larger wave vectors. By tuning with either the size of the seed field or the duration of the experiment, the signal of the contrasting behavior when feedback corrections are taken into account could help investigators to identify the ferromagnetic transition.

One criticism of the recent experiment [3] which reported the first signs of ferromagnetism is that the domains, if present, were too small to image. In the new experimental protocol the pitch length of the initial spin spiral sets the size of the domains formed. However, if this length scale remains below the resolution of the experiment then a statistical analysis of the in-situ phase-contrast imaging could still provide an estimate of the domain size. If the orientation of adjacent domains within a column is independent, then measurements over adjacent columns will give an estimate of the variance of magnetization in each column. The uncertainty in the net magnetization should vary as $sN/4\sqrt{n}$, where s is the spin per atom, N the number of atoms imaged, and n the number of domains. A larger number of domains will result in a smaller variance in the net magnetization, thus allowing the total number of domains to be estimated.

One final experimental probe is spin-dependent Bragg spectroscopy. This could track the decay of the planar spin spiral and the reducing signature at wave vector $\mathbf{P}$. Furthermore, using a variable wavelength optical lattice potential to couple asymmetrically to the spin degrees of freedom, the collective mode response could be studied through dynamical fluctuations of the cloud spatial distribution as a function of wavelength, laser amplitude, and detuning.

VI. CONCLUSIONS

We have studied the time evolution of a spiraling spin texture, prepared by a magnetic field gradient in an interacting degenerate Fermi gas. The linearized dynamics of the magnetization shows an instability, which develops canting out of the spiral plane, with the maximally unstable mode at a wavevector $1/\sqrt{2}$ that of the original spiral. The instability grows exponentially in time with a characteristic time scale that vanishes close to the Stoner transition point. To linear order, the dynamics is the same on the ferromagnetic and paramagnetic sides of the critical slowing down.

Interestingly, however, we find that near the critical point, non linear effects in the dynamics become important. Specifically, scattering of collective excitations on the exponentially growing unstable mode acts to renormalize the spectrum, shifting the instability to larger wave-vectors on approaching the original critical point. Moreover the point of critical slowing is eliminated and the new branch of excitations at high wave-vectors allows a clear distinction between the ferromagnetic and paramegnetic regimes.

Finally, we studied the experimental signatures of the unstable dynamical modes in a realistic trap confinement. Using the calculated dispersion of unstable modes we obtained the spatial distribution of spin-domain sizes in the trap, which may be observed with phase contrast imaging. The most dramatic signature of the new branch of instabilities induced by the non linear feedback effect is a collapse of the domain size at a particular critical radius in the trap.

[*] Electronic address: gjc29@cam.ac.uk

[1] W.C. Stwalley, Phys. Rev. Lett. **37**, 1628 (1976); E. Tiesinga *et al.*, Phys. Rev. A **47**, 4114, (1993).

[2] K.E. Strecker *et al.*, Phys. Rev. Lett. **91**, 080406 (2003); S. Gupta *et al.*, Science **300**, 1723 (2003); C. Chin *et al.*, Science **305**, 1128 (2004); C.A. Regal *et al.*, Phys. Rev. Lett. **92**, 040403 (2004).

[3] G.-B. Jo *et al.*, Science **325**, 1521 (2009).

[4] R.A. Duine and A.H. MacDonald, Phys. Rev. Lett. **95**, 230403 (2005).

[5] I. Berdnikov, P. Coleman and S.H. Simon, Phys. Rev. B **79**, 224403 (2009); L.J. LeBlanc *et al.*, Phys. Rev. A **80**, 013607 (2009).

[6] G.J. Conduit and B.D. Simons, Phys. Rev. A **79**, 053606 (2009).

[7] H. Zhai, Phys. Rev. A **80**, 051605(R) (2009); X. Cui and H. Zhai, Phys. Rev. A **81**, 041602(R) (2010).

[8] M. Houbiers *et al.*, Phys. Rev. A **56**, 4864 (1997); L. Salasnich *et al.*, J. Phys. B: At. Mol. Opt. Phys. **33**, 3943 (2000); M. Amoruso *et al.*, Eur. Phys. J. D **8**, 361

(2000); T. Sogo and H. Yabu, Phys. Rev. A **66**, 043611 (2002); R.A. Duine *et al.*, Phys. Rev. Lett. **104**, 220403 (2010).

[9] D.S. Petrov, Phys. Rev. A **67**, 010703(R) (2003).

[10] D. Pekker *et al.*, arXiv:1005.2366 (2010).

[11] M. Babadi *et al.*, arXiv:0908.3483 (2009).

[12] G.J. Conduit and B.D. Simons. Phys. Rev. Lett. **103**, 200403 (2009).

[13] G.J. Conduit, E. Altman, arXiv:0911.2839 (2009).

[14] R.W. Cherng *et al.*, Phys. Rev. Lett. **100**, 180404 (2008).

[15] G.J. Conduit, A.G Green and B.D. Simons. Phys. Rev. Lett. **103**, 207201 (2009).

[16] A.S. Sorensen *et al.*, arXiv:0906.2567 (2009).

[17] J.H. Huckans *et al.*, Phys. Rev. Lett. **102**, 165302 (2009).